https://doi.org/10.1595/205651323X16685352825345 *Johnson Matthey Technol. Rev.*, 2024, **68**, (1), 161–180

JOHNSON MATTHEY
TECHNOLOGY REVIEW

technology.matthey.com

Recent Developments of Bioactive Glass Electrophoretically Coated Cobalt-Chromium Metallic Implants

Adhesion between bioactive glass coatings and cobalt-chromium substrates

Patrick Munyensanga, Meriame Bricha, Khalil El Mabrouk*
Euromed Research Centre, Euromed Polytechnic School, Euromed University of Fez, BP 51, Main Fez, Morocco

***Email:** k.elmabrouk@ueuromed.org

PEER REVIEWED

Received 9th September 2022; Revised 7th November 2022; Accepted 15th November 2022; Online 15th November 2022

Coating surfaces with bioactive glass can be defined as depositing fine bioactive glasses on biomaterial substrates. Cobalt-chromium is a viable alternative to stainless steel for long-term applications with superior ductility. The mechanical properties of cobalt-chromium alloys are high strength with elastic modulus of 220–2300 GPa, more significant than the 30 GPa of bones. Combining metals and bioactive glass results in high biocompatibility and improved bioactivity of implant surfaces. In addition, it triggers new bone tissue to regenerate through osteogenesis and mineralisation. However, implantation failure still occurs and requires surgery revision due to a lack of adequate bone bonding and delamination at the coating surface of the implant. The current review summarises the adhesion between bioactive glass coatings and cobalt-chromium substrates applied through electrophoretic deposition (EPD).

1. Introduction

Over the decades, traditional metallic biomaterials such as stainless steel, cobalt-chromium, titanium and its alloys have become the standard implant biomaterials for load-bearing in hard tissue applications (1). However, their low biocompatibility and degradation rate *in vivo*, as well as their lack of significant bioactivity and other biological functions, make them vulnerable in biomedical applications. Biodegradable metals, such as magnesium, iron and zinc, are found in these vulnerable areas *in vivo.* Thanks to advances in biomedical research, bioactive glasses and ceramics have been introduced to form soft tissues, as well as widely used as coating biomaterials on load-bearing metallic implants (1, 2).

A biomaterial may be considered suitable *in vivo* when it possesses desirable bioactivity. An example is a bioactive orthopaedic implant that allows bone induction and cell proliferation for osteoinduction. Another example is a cardiovascular implant that stimulates the formation of blood vessels for angiogenesis and antibacterial activity. An advantageous property for implant surfaces explains biofunctionalities of the outer shell that integrates healthy implants within the host.

Fibrous biomaterials can develop at the interface and lead to loosening and undesirable toxicity within the host and eventually, failure of the implants (3–6). To overcome this failure, aspects such as a core metal implant coated with a biomaterial that is highly biocompatible are

considered. This will integrate within the host human tissues better than other biomaterials. Another aspect is mineralising apatite formation at the interfaces, which enables bioactive glasses to assist metal implants in integrating better into the host. They can also control or prevent implant failure such as corrosion in the biological environment and can stimulate tissue regeneration and degradation at a similar rate (7).

The third aspect is the need to consider the interaction of the biomaterial with the biological system at the nano-level while designing medical devices. This aids in the osseointegration process. The short process has been summarised during the initial implantation stage (8). The authors described the process from a microscale viewpoint, where inflammatory cells such as monocytes, lymphocytes and granulocytes of white blood cells arrive first to contribute to the healing process near the wound surface. The primary blood components such as plasma, platelets, red blood cells and white blood cells interact with many proteins associated with host inflammatory response and communicate with the implant's outer layer surface when released.

On the other hand, released cells require an intermediary layer made up of adsorbed water molecules, followed by protein and lipid receptors from the blood, which promote cell adhesion to the implant surface at the nanoscale. To successfully connect the cells to the implant surface, a layer of adsorbed water molecules is needed under which a new layer is formed. The layer is apatite, allowing the cells to connect to the implant surface successfully, thus stimulating osteoblasts for new bone formation (8, 9). These aspects might be explained as *in situ* biomineralisation coating.

After implantation, various physiological response reactions occur and the implants' performance depends on the interfacial outer surface. If it falls below a specified acceptable level, considerable adverse effects emerge, resulting in implant loosening or surgical revision. Priyadarshini *et al.* summarised various factors, primarily the root cause of this failure. These include particulate matter and debris from ions (caused by corrosion or wear), fibrous encapsulation (caused by insufficient bone integration or osteointegration), inflammation, low fracture toughness, low fatigue strength, variations in the modulus of elasticity of the implant material and the surrounding bone (stress shielding) and infection (10). In addition, if the coating layer around the implant that has undergone surface modification is extremely thin, the host system will have an easier time tolerating it and fewer corrosion products will be generated (11, 12).

Implant surface treatment is crucial. It defines the biofunctionalities of the implant, as shown above. Thus, it is essential to understand the structure design of surface functionalisation through the coating to explain the adsorption and cell adhesion processes that tend to mechanically invade the outer layer formed at the interface between the tissue, coating specimen (bioglass) and implant core surface. Shrinkage of this surface from biological reactions accompanied by mechanical stresses between the implant surface and host tissues define the adhesion strength and chemical stability of bioglass-coated implants.

Fortunately, a well-known coating technique, EPD, deposits functionalised materials such as bioactive glass and hydroxyapatite (HA) on metallic implants (13). It has a key advantage compared to other coating techniques (**Table I**) due to its cost-effective, simple process setup and ability to deposit coatings at room temperature (4, 14, 15). Therefore, the technique is an attractive coating method to deposit bioactive glass and ceramics to metallic and polymer implants for various biomedical applications. Two-step phases occur during the process: electrophoresis, which consists of moving charged particles in suspension under the influence of an electric field; and desposition on the oppositely charged electrode to form a dense coating.

Subsequently, coating characteristics and quality are measured against their porosity, oxide content, macro-micro hardness, bonding strength and surface roughness (16). In addition, obtaining homogeneous and highly adhesive coatings requires a well-dispersed suspension. Thus, both suspensions and physical parameters of EPD determine the quality of bonding between core and bioglass coating. EPD also offers possibilities of coating complex materials of three-dimensional (3D) or porous structures while producing free-standing objects. However, the strength of bonding between the core substrate and bioglass requires further heat treatment (sintering) to densify the coatings due to the colloidal process of EPD (16, 17).

This review describes relevant metallic implant biomaterials, the EPD technique and coating quality parameters. In addition, mechanical strength, bioactivity, adhesion strength, chemical stability and surface functionality of cobalt-chromium-coated bioglass materials are discussed. The review also intends to provide specific technical aspects

Table I Implant Coating Characteristics and Properties of Electrophoretic Deposition Compared to Other Known Processes (4, 14, 15)

Sol-gel	Biomimetic process	Pulsed laser deposition	Electrophoretic deposition
High sintering temperature for HA coatings	Low temperature	High temperature	Low temperature
Combination of processes	Different types of substrates	Amorphous phase of substrates	Conducting substrates
Substrates with complex geometry	Induced HA metallic implants	Chargeable dense particles	Chargeable particles
Biomaterial substrates	Bioceramics and polymers	3D crystalline coatings	3D rapid deposition
Thin film	3D Crystal structure	Incorporation of biological agents	HA and ion-doped HA
3D control of composition	Ion-doped HA	Thick and cracked coatings	Significant bonding strength
–	Low bonding strength	–	Uniform coating thickness
–	Porous structure	–	–

of the cycle effects parameters of bioactive glass particles within the suspension and discuss their mechanisms. The summary and outlook highlights the ambiguity raised in the literature about cobalt-chromium and related biomaterials over their chemical history.

2. Cobalt-Chromium with Other Metallic Implants

Cobalt-chromium and stainless steel are two biomaterials known to be used during the twentieth century in orthopaedics applications. They both belong to the same classification of traditional metallic biomaterials, which include stainless steel, titanium, cobalt-chromium and their alloys and play major roles as load-bearing implants. The second classification, for hard tissue biomaterials, forms biodegradable and bioresorbable biomaterials used for wound healing, including zinc, magnesium and iron. However, in several studies, the bioresorbable materials are observed to degrade at a controlled rate *in vivo* application (18). This routine is regraded to functionalise implants based on primitive purpose under these three significant chemical elements steps to enhance good biocompatibility and implants' mechanical functionalities properties. Therefore, we might find alloying design a novel structure design and surface modification (19, 20).

Stainless steel, commonly used as a biomaterial, is involved in repairing cardiovascular stents and valves, especially 316L stainless steel, which is rigid with good fatigue strength, ductility and hardness. However, it has been replaced by titanium and Ti-6Al-4V alloy for dental implants due to their light weight, high strength, low density and excellent corrosion resistance (21). Titanium alloys are selectively used in biomedical applications due to their bioinertness that gives them good biocompatibility. They can also form a stable oxide layer on their surfaces and stimulate bonelike apatite formation (1).

Cobalt-chromium alloy is similarly selected due to its good mechanical properties, high ion corrosion resistance, low wear performance and biocompatibility. It is widely used in biomedical engineering applications such as metal-on-metal hip resurfacing joints. It is suitable owing to its cobalt and chromium content, molybdenum and other trace elements (22–24) (**Table II**). However, unlike austenite and AISI 316L stainless steel, after several failures, both are discarded because of the chemical content of nitrogen, which accelerates corrosion and results in high friction, a large number of wear debris particles and leads to a rapid loosening of implants. This was the main reason cobalt-chromium was introduced in orthopaedics for various applications (25). However, manufacturing challenges limit it to specialised processes and applications (26). Also, as previously studied, close contact during the implantation of chromium and cobalt cause metals to leach into the bloodstream and exhibit toxicity (27–29).

Haynes *et al.* used rats *in vivo* to compare the toxicity and release of titanium grade five and cobalt-chromium from metal-on-metal implants (30). They concluded that a titanium-aluminum-vanadium alloy implant leached

Table II Commercial Cobalt-Chromium Alloys (22–24)

Alloy	Nominal chemical analysis of rod											UNS[a]	ASME[b]/ AWS[c]	Hardness, HRC
	Co	Cr	W	C	Ni	Mo	Fe	Si	Mn	O	Others			
Stellite 1	Bal.	32	12	2.45	<3.0	<1.0	<3.0	<2.0	<1.0	0.003–0.2	<0.5	R30001	(SF) A5.21ErCoCr-C	51–56
Stellite 6	Bal.	30	4–5	1.2	<3.0	<1.0	<3.0	<2.0	<1.0	0.003–0.2	<0.5	R30006	(SF) A5.21ErCoCr-A	40–45
Stellite 12	Bal.	30	8	1.4–1.8	<3.0	<1.0	<3.0	<2.0	<1.0	0.003–0.2	<0.5	R30012	(SF) A5.21ErCoCr-B	46–51
Stellite 20	Bal.	33	16	2.45	<3.0	<1.0	<3.0	<2.0	<1.0	0.003–0.2	<0.5	–	–	53–59
Stellite 21	Bal.	28	–	0.25	3	5.2	<3.0	<1.5	<1.0	0.003–0.2	<0.5	R30021	(SF) A5.21ErCoCr-E	28–40*
Stellite 22	Bal.	28	–	0.30	1.5	12	<3.0	<2.0	<1.0	0.003–0.2	<0.5	–	–	41–49*
Stellite 25	Bal.	20	14	0.1	10	<1.0	<3.0	<1.0	<1.0	0.003–0.2	<0.5	–	–	20–45*
Stellite 31	Bal.	26	7.5	0.5	10	–	<2.0	<1	<1.0	0.003–0.2	<0.5	R30031	–	20–35*
Vitallium	64.8	28	–	0.25	–	5.58	–	0.75	0.7	–	–	–	–	35

[a]Unified Numbering System (UNS); [b]American Society of Mechanical Engineers (ASME); [c]American Welding Society (AWS)

particles and generated a substantially greater prostaglandin release than cobalt-chromium particles. Furthermore, the presence of titanium alloy particles elevated interleukin-1, interleukin–6 and tumour necrosis factors. On the other hand, chromium-cobalt alloy particles inhibited the release of prostaglandin E2 and interleukin-6 but had no impact on interleukin-1 or tumour necrosis factor (20, 30). As a result, it is reasonable to claim that cobalt-chromium is a better alternative for major joint replacement applications than titanium and its alloys (1).

3. Physiochemical Properties of Cobalt-Chromium and Bioactive Glass

Cobalt-chromium and its alloys have been widely used in biomedical applications. They are known to have increased inhibition against corrosion by creating an oxide layer (such as Cr_2O_2) on the core surface through the passivation process in its α-phase. This process is found in 316L stainlesss steels with chromium particles in their composition. However, the carbon content in stainless steel alloys decreases the implantation period to less than 13 years due to the release of metal ions with an increased concentration of carbon into body fluid. Therefore, these reactions lead to systematic inflammation and implant loosening (31). For comparison, various properties must be investigated, some of which affect how implants delaminate. Consequently, some related to the process and composition at the synthesis stage are discussed here.

3.1 Chemical Exfoliation Compound

Since the human body is highly corrosive, stringent requirements are imposed on the candidate materials' properties. Biomaterials must be inert and it is necessary to study their corrosion behaviour in contact with body fluids (32). An example of cobalt-chromium alloys is to create better candidates by tailoring their content. Their high corrosion resistance even in a chloride environment and high concentration of cobalt of 58–70 wt% and 26–30 wt% of chromium with a small number of other metals (see **Table II**) make cobalt-chromium viable choice biomaterials for long-term application with good ductility and with a minimum elongation of 8%. The mechanical properties with high-strength biomaterials of elastic modulus of 220–2300 GPa, greater than the 30 GPa of bones, provide good fatigue strength and wear resistance in artificial hips or knee replacements. However, similar to other metallic biomaterials, cobalt-chromium with molybdenum and nickel ion content leads to carcinogenic (nickel ions) and allergic reactions (molybdenum and cobalt ions), as well as the correlation between neurotoxicity and several neurogenerative diseases such as Alzheimer's and Parkinson's. It has been reported similarly for stainless steel and other metal implants

such as aluminium, copper, vanadium, arsenic and lead (33, 34).

3.2 Cobalt-Chromium Biomaterials *in vivo* Trials

The literature does not provide all information about the neurotoxicity of cobalt-chromium degradation particles in body fluid nor the clinical indications of toxicity in patients with total hip replacements (25, 35–37). Between 2003 and 2011, it was reported in the UK that at least 31,171 metal-on-metal hip implants were subject to failure that were recalled for revision. Furthermore, a study by Green *et al.* presented ten cases of men aged in their 60s. They evaluated the neuropsychiatric morbidity due to metal-on-metal hip implants failing from 2005 to 2009 for acetabular, taper sleeve adaptor and unipolar femoral implantation. The result revealed a mean level of chromium of 338 nmol l^{-1} and meant cobalt level of 669.4 nmol l^{-1} after revision of implants following neuropsychiatric complications due to cobalt-chromium toxicity. In addition, most neurocognitive and depressive deficits were discovered to be due to cobalt-chromium metallosis (36). Bijukumar *et al.* also conducted a study with the help of a hip simulator investigating disruption of DNA replication dynamics in neuronal cells due to the degradation products of cobalt-chromium alloy nanoparticles (NPs).

The level of toxicity in neurons was compared from degradation products against processed degradation products washed with phosphate buffered saline during the process. The results indicated that degradation products have more DNA damage in double and single-stranded breaks and alkaline labile DNA adducts processed degradation products (34). However, degradation products were found to be more bioactive compared to processed degradation products, thus suggesting further consideration of the toxicity level evaluation of cobalt-chromium implants. Other studies confirm corrosion due to cobalt-chromium molybdenum ions released into body fluid which is more toxic than that of 316L stainless steel. In low bonding failure and inadequate adhesion strength between the bioactive glass and the metal substrate, metal implants cause stress shielding and bone loss over time. This resulted in delayed healing and decreased bone strength (38).

Furthermore, upon prolonged accumulation of metal ions in the blood, there is a higher risk of metal accumulation in organs affecting the normal functioning of these organs and resulting in organ failure. Thus, metallic materials are not entirely accepted by the body and tissue growth is impaired due to insufficient attachment of the implant, leading to discomfort or pain. Studies have explained the biofunctional failure of cobalt-chromium alloys by the presence of nickel, molybdenum and chromium ions. When released, these elements are recognised as toxic to human bodies, leading to the accelerated biocorrosion of implants as well as the development of skin-related diseases. Organs such as the kidney, liver, blood cells and lungs are among those affected by excessive leaching of cobalt-based alloys (39, 40). Thus surface modification of cobalt-chromium implants is needed to meet requirements for high biocompatibility and good bioactivity (10, 34, 35).

3.3 Thermal Expansion Coefficient of Bioactive Glasses Coated

There is a large amount of literature data on the orthopaedic applications of highly bioactive and biocompatible materials. Bioactive glasses as biomaterials can bond to bone tissues and form a bonelike mineral apatite-hydroxyapatite (HP) at the surface when in contact with physiological fluid. Therefore, bioactive glasses are frequently used as composite materials or coating layers, improving metallic implants' biocompatibility. However, the ability to bond with a metallic substrate or a second phase depends strongly on the coefficient of thermal expansion (CTE), which controls the formation of thermal residuals (41). This can be seen as a drawback of bioactive glass coating deposition due to low adherence with the core substrate. Garrido *et al.* suggested different strategies to overcome this low adherence throughout bond coats. It includes modifying the glass composition (doping synthesised bioactive glass), using glass-based coatings, titanium oxide, lithium oxide, barium oxide or blends like chitosan and glass–ceramics or pre-heating the substrate (42).

The thermodilatometric compatibility of bioactive glass coatings with the substrate regulates the formation of harmful thermal stresses at the interface. Accordingly, it significantly impacts their dependability, notwithstanding the importance of the CTE of bioactive glasses. The thermal expansion, if mismatched or higher than that of bioactive glass, which is usually in the 14–15 × 10^{-6} K^{-1} range, leads to the creation of significant residual tensile stresses in the glass coating layer. This might cause fracture development and poor interface adhesion regardless of the deposition

process. A coating material's CTE might be relatively lower than the substrate's, producing desired compressive stresses in the glass coating and improving the mechanical durability of a quasi-brittle coating (43–45).

Several effects of CTE on the thermal shock resistance of glass are typical and usually withstand high thermal stress. It happens when possessing a small thermal expansion coefficient. Moreover, the CTE improves glassware's time-temperature and cooling schedule. While designing specific glass products, it is also necessary to consider the required variable temperature conditions that affect the CTE (46). This offers the control to design high-quality glass coating and composite compounds. Most significantly, the characteristic of thermal expansion below the glass transition depends on the asymmetry of thermal vibrations in the glass structure. On average, strong bonds in the glass network result in low amplitudes and lower CTE values (41, 46).

3.4 The Effect of Modifier Oxides and Intermediate Oxides

Several analytical methods estimate the CTE of glass based on its composition. However, they have been formulated for generic glasses, not specifically for bioactive glass. After implantation, bioactive glass with good composition experiences a controlled release of ions *in vivo*, such as silicon and phosphorus and regulates gene transcription (4), which promotes cell proliferation and regenerates new bone tissues. Moreover, it results in bioactive glasses' diffusion in orthopaedic spinal, craniomaxillofacial and periodontal application. The capability of bioactive glasses, which can be used for drug delivery in soft tissues, is explained by the controllability of their composition enabling toxicity to be modified (6).

Particular formulations of bioactive glasses are distinguished by the adjustment of CTE estimation models that improve predictivity of the coating up to deposition. As previously studied, thermal expansion below the glass transition usually depends on the asymmetric amplitude of thermal vibrations in the bioactive glass compositions. Strong bonds in the glass networks undergo crystallisation behaviour resulting in small amplitudes, reducing the CTE values. An example of strong bonds in glass networks was observed by Mohan Babu *et al.* (47). The investigation of physicomechanical and spectral studies of Zn^{2+}-doped P_2O_5-based bioactive glass produced results consistent with previous research, which demonstrated a decrease in molar volume due to a drop in the mole fraction of oxygen ions of the samples (48). Consequently, the decrease in molar volume was attributed to the greater binding strength of Zn–O bonds compared to P–O–P and P–O bonds resulting in shorter bond lengths, leading the glass network to tighten (47, 49, 50). This is also explained by the use of silica coatings to allow more straightforward surface modification to inhibit the HA layer. Below is the general additive Equation (i) that predicts the effect of oxides on the CTE of bioglass:

$$CTE = \Sigma_{i=1}^{n} \alpha_i p_i \quad \text{(i)}$$

where α_i is proportionality factor, based on several models available; p_i is weight fraction of corresponding oxides with a corresponding number of constituents in the glass (n).

Note that the α_i factor can be calculated upon the values of a mathematical model of Winkelmann and Schott, while others can be based on empirical results, especially those that English and Turner referred to as a value in the range 25–90°C. Similar to Gillard and Dubrul, with a value range between 37–55°C and the Hall model from 25°C to the lower limit of the critical temperature of the analysed glass (41, 51). A detailed summarised table can be found in the original articles of Fluegel (52) and Bellucci *et al.* (41).

Equation (i) is significant; however, it is based on heat treatment to fix adhesion forces of bioactive glass on coated substrates (1). Several parameters may be relevant to this additive Equation (i), as described in the study of Fluegel (52). The amplitude of asymmetric thermal vibrations is the root cause of thermal expansion depending on the temperature change; if L_o, the original length of the sample at the reference temperature and L, the length of the sample at a temperature, T, are varied, then the possibility to define the expansivity α is obtained in Equation (ii):

$$\alpha = \frac{dL}{L_o dt} \text{ and the } CTE = \frac{\Delta L}{L_o \Delta T} \quad \text{(ii)}$$

where (dL) stands for the infinitesimal length change that corresponds to the infinitesimal temperature change of (dt); and (ΔL) is the length change caused by temperature change ΔT. The analysis of both relations explains if $\Delta T \rightarrow 0$, $\Delta L \rightarrow dL$ and $CTE \rightarrow \alpha$. This means the expansivity increases with increasing temperature. Thus the CTE increases with increase of ΔT. If it is fixed at a higher temperature, as described in most relevant studies referring to intervals of 20–300°C or 100–300°C even if it is not standard procedure (52).

According to Fujino *et al.*, incorporating various trace elements in the glass composition is

recommended to achieve CTE similar to the core substrate (38). Some effects include K_2O and MgO acting on the modifiers to create an intermediate oxide based on the glass transition temperature, as concluded by O'Donnell (53). Thus, CTE is modified by adding various functional oxides to the glass composition and is frequently related to the relative amount of oxide. An example was the capacity for glasses in the family of 45S5 Bioglass® systems to attach to bone tissue. Three factors in the process are: (a) a low silica content (typically less than 60 mol% for melt-derived glasses); (b) a high content of network modifiers; and (c) a high Ca:P ratio (54). Under this assumption, each oxide in a bioactive glass composition has a direct and predictable effect on the CTE of glasses, formulating the general additive equation and estimating their thermal ability for post-heat treatment.

3.5 The Porosity of Bioactive Silicate Glasses Coated *via* Electrophoretic Deposition

The porosity of a neat powder-coated surface is represented by a small bubble with holes filled with air. They are characterised by microscopic analysis. A coated surface with porosity appears to be bubbling out on the sharp end of the film and seems to be a speck of black dust. The porosity of a final coated surface can consequently be derived from the substrate at its surface, which has existing metal porosity or microporosity in a powder coating. According to previous studies (55, 56), trapped air or contaminants on the substrate are the most prevalent source of porosity in a powder coating layer. The porosity might come from a powder formula containing components that migrate off the film and cause minor depressions during the coating process (57).

In addition, the successful functioning of a bioglass-coated prosthesis or other orthopaedic implant depends on the strength of the bond between glass and bone as well as the glass coating and metal substrate (58). Farrokhi-Rad *et al.* studied the effect of controlled porosity during EPD of a HA nanostructure on a sacrificial template that is a porogen agent of a carbon black (CB) (59). As a result, CB-HA has a positively charged surface with coarser and finer surfaces. At the beginning of EPD, the deposition rate from suspensions with a concentration ratio (CB:HA ratio) of 0.25 was faster than those with 0.5. However, the condition was inverted for more extended EPD periods. It was also discovered that the amount of porosity in the coatings increases as the CB concentration in the suspension increases, with coatings deposited from suspensions containing 20 g l^{-1} of HA nanoparticles. Adjustment of the CB particles was as follows: 0 g l^{-1}, 5 g l^{-1}, 10 g l^{-1} and 20 g l^{-1}, having 15%, 24%, 31% and 43% of porosity, respectively.

Correspondingly, a flame-spray method was developed to prepare a uniform coating of 45S5 Bioglass® on a stainless steel substrate without post-heat treatment to soften the bioglass on the substrate. However, the coating was not entirely successful due to porosity at the glass-metal interface, as the molten glass particles struck and fused to the metal surface. Porosity at contact remained an issue and *in vitro* studies revealed that the coating had low fatigue strength and significant corrosion at the glass-metal interface. Similarly, after being implanted in monkeys, several flame-spray-coated implants failed *in vivo* (58). Metals such as 316L surgical stainless steel, titanium or cobalt-chromium alloys have numerous benefits over other metals for bioglass-coated implants. Some include good fatigue strength in physiological environments with thermal expansion close to that of bioglass formulas: 13–16 × 10^{-6}°C^{-1} compared to cobalt-chromium of 12 × 10^{-6}°C^{-1} (60). Core implants with unique, novel structures, including porous, nanostructured and glassy materials, provide various options for biomedical applications.

Compared to previous procedures, surface modification is more common and frequently used to change the surface topology, chemical composition and wetting behaviour. Through suitable surface modifications, the surface becomes biocompatible and bioactive with improved properties (4, 61). These surface modifications might be transferred to suitable bioactive biomaterials as a coating on metallic substrates (62, 63).

4. Functionalisation of Electrophoretic Deposition

4.1 Silicate Bioactive Glass in Coating Techniques

Silica materials have been used as a shell to protect the inner core of a biomaterial from air degradation; such instances resulted in corrosion. It has also been used as a network modifier of the particle castoff to improve biocompatibility and allow easy surface modification (64, 65). Various techniques have been used at the synthesis stage. Microwave irradiation was involved in producing homogeneous heating and protecting a wide range

of cores with silica. In post-heat treatment, these techniques were used to include dopants such Ag^{+}, Mn^{2+}, Zn^{2+} on silica and produce particles aggregated into a thicker sphere shell (66).

Previous studies confirmed different techniques used to create 45S5 Bioglass® coatings onto titanium implants (67, 68), cobalt-chromium alloys and other metallic implants (58, 69, 70) as well as polymers (71). Such coating techniques as sol-gel (63, 72), plasma spraying (73), laser cladding (68) and EPD (58, 62) have been used. Each technique has its advantages based on the application environment.

4.2 Surface Preparation and Pre-Coating Techniques

The EPD is a facile coating technique with a controlled thickness characterised by a uniform coating and high-purity deposition. EPD is of increasing interest for bioglass coating deposition onto bioinert metallic materials from one-phase transformation during coating. It offers advantages such as obtaining high-purity coatings at low cost and can be applied to oversized and complex-shaped implants, including porous structures (74, 75).

Functionalising EPD includes the migration of charged particles (see **Figure 1**) in an electrolytic solution and gives EPD the ability to form homogeneously dispersed powder particles in an aqueous or non-aqueous medium for anode or cathode (16). A controlled coating layer thickness is obtained resulting from moving charged bioglass NPs in liquid suspension by applying an electric field under coalescence deposition. **Table III** illustrates different parameters involved in obtaining a layer thickness typically measured between <500 µm and ≤1 µm (76).

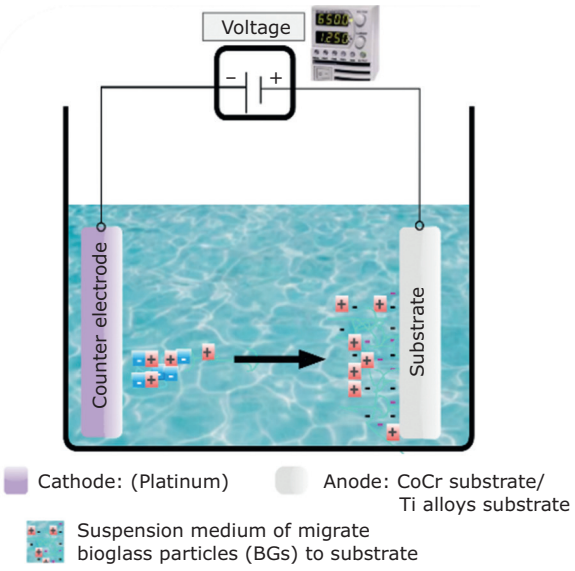

Fig. 1. Electrophoretic deposition sketch

Pre-coating techniques can be used to ensure the homogeneity of surface coatings. Surface preparation can be carried out using grit blasting with a mixture of oxides such as alumina and glass beads, then ground and dried with 240 grit silicon carbide paper. More details on these techniques can be found in the research of Lacefield and Hench (58). Another method is to functionalise the pre-coating surface and reduce contaminants. Unfortunately, this leads to a porous-coated layer (undesirable micro-sized bubbles) when a core surface is electropolished in perchloric acid or is ultrasonically cleaned in acetone.

It is possible to alter the surface properties of a surface by suspending low surface energy particles in a solvent. As particles agglomerate in suspension, they are subjected to electrophoretic deposition onto a substrate for a predetermined amount of time. The altered surface may be superhydrophilic or superhydrophobic. Therefore, a rough layer of particles can be applied to the surface to provide texture or roughness to the surface. A substrate surface can be fully functionalised by subjecting it to a suspension of particles mixed with a bonding additive for electrophoretic codeposition onto a substrate with various solvents (77) such as ethanol, butanol (78, 79) or isopropanol (59, 67). The method is similar to dip coating but with a pre-coating process, as described in Lacefield and Hench's study (58). According to Farhadian *et al.*, three different procedures (**Figure 2**) sufficiently prepare the surface for EPD (80). Throughout these procedures, the surface energy was enhanced by mechanical polishing using silicon carbide papers up to 1200 grit, anodic oxidation to create porous surfaces and electrochemical polishing to create an atomically-clean surface. Therefore, both the roughness and surface chemical composition of 316L stainless steel were modified through anodic oxidation treatment and roughness values were also improved (**Figure 2**). A similar method has been used to fully functionalise the surface of cobalt-based alloys resulting in increased surface energy and superior surface irregularities and cavities (81, 82).

Table III Electrophoretic Deposition Particles Functionalise Surface Coated Layer (Primer)

Suspension parameters	Reference	Physical parameters	Reference
Particle size	(83)	Voltage deposition (Constant or dynamics)	(119)
Dielectric constant	(16, 120)	Deposition time and temperature	(38)
Conductivity and zeta potential	(84)	Substrate conductivity	(119)
pH of electrolyte	(71)	Density of substrate	(79, 97)

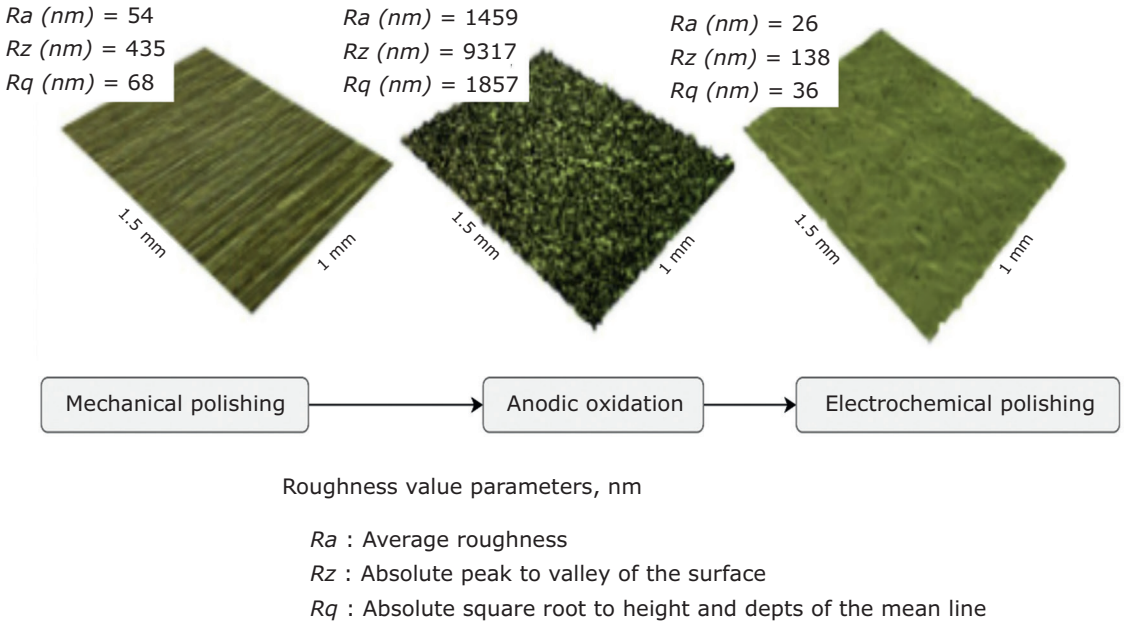

Fig. 2. Microscopic images of various procedures illustrating a treated surface of 316L substrate (modified from the author (80) with permission from the publisher)

4.3 Bioactive Glass Suspensions for Electrophoretic Deposition

A technique to achieve stable charged particles in suspension is essential for the efficiency of EPD. The concentration of suspension, stability, pH and size of the suspended species have to be controlled because all directly impact the uniformity, density and roughness of the resulting deposit layer. EPD has used both aqueous and non-aqueous solutions. Various studies analysed the behaviour of particles in suspension. Lower surface charged particles tend to attract each other and the deposited coating results in a porous surface, while particles with a highly charged surface produce a strong electrostatic repulsion force and result in a reduced deposition time to get a dense coated surface. Hence, a uniform particle suspension with proper conductivity in medium dielectric gives a coarse coating layer (16, 83). Extensive research was conducted (38) to establish the best glass composition and firing parameters (temperature and duration) to fabricate homogenous coatings with good adherence to cobalt-chromium alloy. The study ended with a coating thickness range between 40–60 µm.

Glasses prepared with melt quenching techniques were coated on cobalt-chromium alloy and only 6P50 glass composition $49.8S_iO_2$-$15.5Na_2O$-$4.2K_2O$-15.6CaO-8.9MgO-$6P_2O_5$ was successfully fabricated to yield transparent, dense coats without any delamination or presence of crack defects on the finished parts. A firing temperature of about 750°C was used for 30 s to obtain good adhesion by forming a CrO_x layer with 150 nm thickness at the glass-metal interface. The suspension was a mixture of glasses of particle size <20 µm with ethanol. This shows the possibility of successfully coating silicate glass onto cobalt-chromium alloy and the ability to form hydroxyapatite ($Ca_{10}(PO_4)_6(OH)_2$) on the interfacial surface of the glass layer in 30 days of *in vitro* testing with simulated body fluid. The study demonstrates optimum capability to achieve excellent adherence

and good bioactivity. The CTE and softening temperature (T_s) contributed to identifying the firing temperature used in the adhesion of glass to the metal interface. Suspension stability is also obtained with a better deposited coating at the desired thickness on the substrate.

4.4 Kinetics and Challenges Involve Coating Metallic Substrate with Bioactive Glass

Coating complex-shaped biomaterials is challenging when using frit enamel rather than immersion coating techniques such as sol-gel coating. However, coating biomaterials could be more easily accomplished by dipping a substrate into bioglass NPs within a frit solution and then sintering the frit layer to form a smooth glass coating. Understanding EPD and its kinetics process allows the characterisation of final films. Hamaker's law (84) is used to obtain efficient parameters. This is a well-known mathematical model that helps to predict those parameters properly. The kinetics of EPD indicates a relationship between electric field strength (dielectrically constant) and deposition yield. It is similar to coating quality, which is determined mainly by conductivity and zeta potential, as well as particle size within the suspension.

$$m(t) = \int_{t_0}^{t} \mu C_s S E dt \qquad \text{(iii)}$$

Equation (iii) helps predict the deposition of the layer prepared for the co-deposition of EPD. It also helps to evaluate processes relative to the theoretical values of NPs present in suspension and determines electrophoretically deposited mass, *m*, in grams from electrophoretic mobility, Equation (iv):

$$\mu = [cm^2.s^{-1}.V^{-1}] = {}^{v}/_{E} \qquad \text{(iv)}$$

Electrophoretic mobility presented in Equation (iv) represents the velocity, *v*, of particles moving in suspension under the influence of applied field strength for zeta potential of glass loading, C_s g cm^{-3}, intended surface area, S cm^2, to cover; and electric field strength, E V cm^{-1}, as well as time, *t* s (16, 84). The Hamaker equation may be used to qualitatively characterise the connection between deposit mass, deposition time and voltage. By integrating the equation over time, Equation (iii) is obtained, which predicts a linear rise in deposited mass as the electric field (**Figure 3(a)**) and deposition time increase, where the mass (M) of a deposition is formed on the electrode area

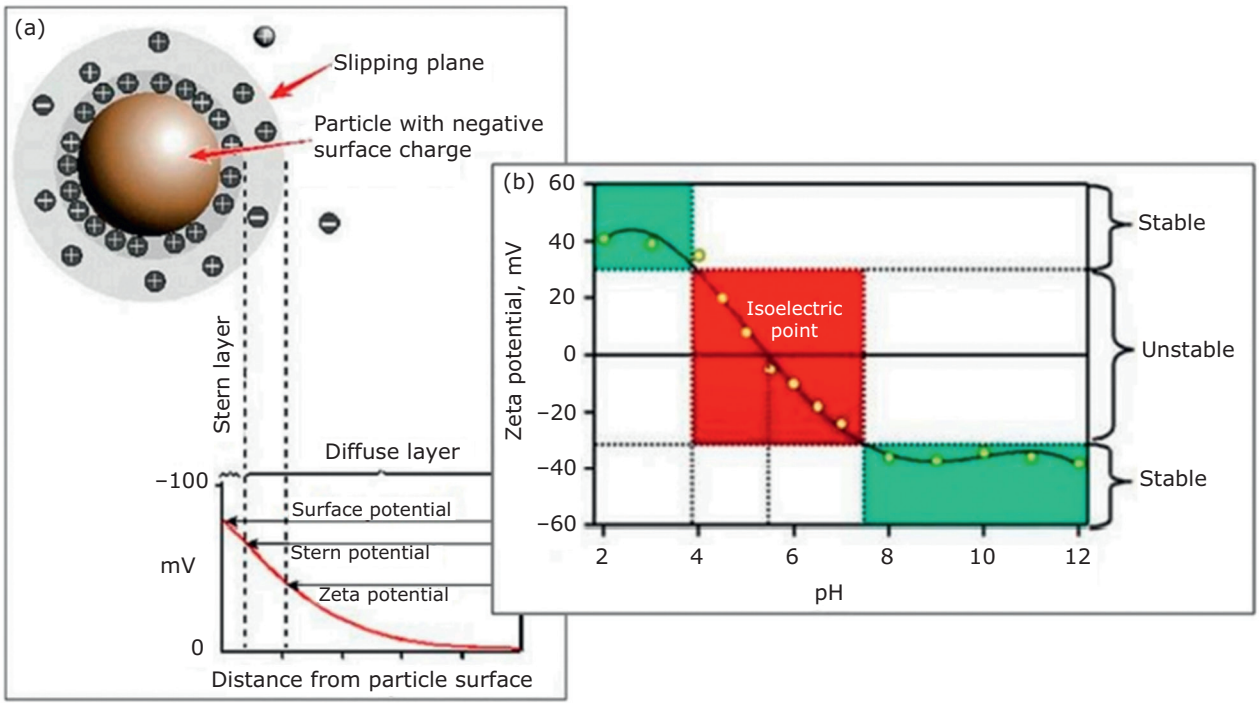

Fig. 3. (a) Schematic representing Zeta potential; and (b) zeta potential *vs.* pH plot showing the values of conditions on which stable or unstable suspensions are formed. Reproduced from (86) under the Creative Commons BY-NC-ND license terms

(S) during deposition time, due to suspension concentration (C) and electrophoretic mobility.

$$M = \mu SCET \quad (v)$$

However, a minimum electric field is required to overcome repulsive interparticle interactions. Low voltages can cause reduced deposition (85). This too-low voltage causes the particles to move to the electrode surface, but their interparticle repulsion will not allow them to aggregate and make a deposit. The explicit deposit formation process is complex and different mechanisms have been suggested. For example, as discussed in this section, charge neutralisation of particles at the electrode surface must come from local pH variations originating from EPD.

The pH of the suspension is one of the critical elements affecting the zeta potential, as seen in **Figure 3(b)**, illustrating suspension in an aqueous medium. For a suspended particle with a negative zeta potential, the particles tend to become increasingly negatively charged when additional alkali is added. The suspension will eventually reach a point where the charge will be neutralised if acid is introduced to it. In addition, if the ions are mainly adsorbed, more acid addition may result in a build-up of positive charge. The zeta potential *vs.* pH will show a positive slope at low pH and a lower or negative slope at high pH. Therefore, suspension stability is optimised when considering the intermolecular interaction, which is measured by measuring the zeta potential of the solutions and their pH values. Ma *et al.* stated that a zeta potential of ~+30 mV gives sufficient physical stability to suspension (16, 87, 88). As in Ahmed *et al.*, the suspension of zein/bioactive glass did not show any sign of sedimentation during EPD when zeta potential 30 ± 5 mV and pH 3 were used (89). This confirmed previous studies and gave insight into the effect of the zeta potential on suspension stability. Studies show that zeta potential measurement proves the electrokinetic behaviour of bioactive glasses based on their stoichiometry. The positive and negative zeta potentials in both acidic and alkaline suspensions are associated with the ions of the glass NPs. Therefore, the deposition mechanism is accelerated by electrokinetic properties, while the ionic strength, pH and concentration of suspensions affect this mechanism and the particle size (59) and shape morphology of the bioactive glass (90–92). Thus, grinding is required to reduce the size distribution of NPs drastically and improve suspension stability for the EPD process. **Figure 4** illustrates the wet grinding technique for reducing particle size distribution (67).

The isoelectric points (IEPs) were proven to be affected by synthesis conditions and IEP 4 from HA-prepared suspensions was found in samples prepared under more acidic conditions, while values ranging from 5.5–7.2 were found in alkaline suspensions in precipitated HA (93). The IEP in **Figure 3**, particularly significant from a practical perspective, is found where the plot crosses through zero zeta potential. Thus, the colloidal system seems to be least stable at this point because aggregation was most probable (86). Additionally, post-heat treatment significantly affected the coat adhesion mechanism to the substrate (**Figure 5**). In any case, the coated surface will fail when the firing temperature exceeds the T_g of the glass. This is because the coated surface is crystalline and almost completely crystallised at the lowest temperature. For example, Fujino *et al.* used a firing temperature above 800°C (**Figure 5(b)**), but the coated surface resulted in poor densification and lack of adhesion, leading to crack propagation in 6P50 and cobalt-chromium substrates during the indentation test (38).

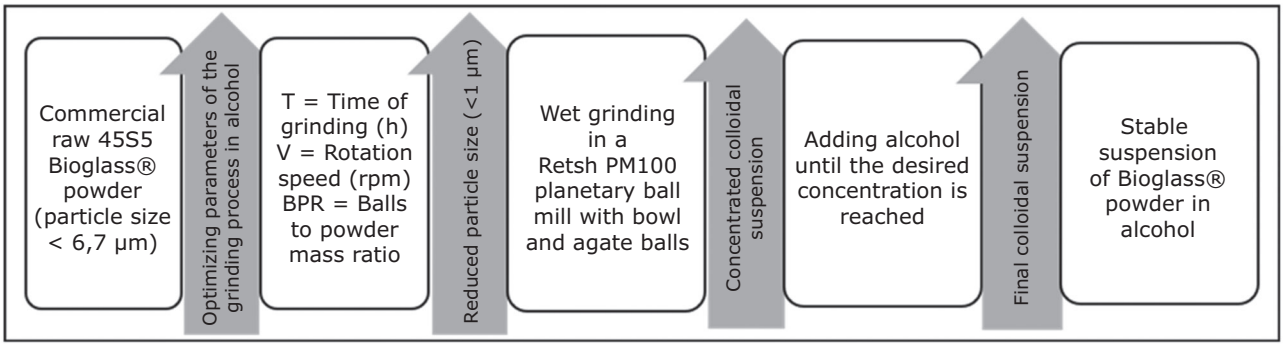

Fig. 4. Schematic illustration of the wet grinding process of bioactive glass, type of 45S5. Reproduced from (67) under the Creative Commons BY-NC-ND license terms

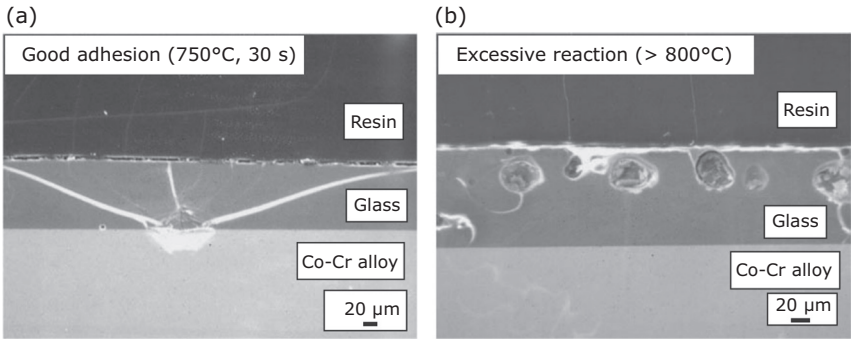

Fig. 5. Illustration of: (a) coating surface cross sections of 6P50 and cobalt-chromium substrate; and (b) porous coated surface with poor adhesion due to excessive reaction from thermal heat treatment of coat at >800°C, 5 min. (Reprinted from the author (38) with permission from the publisher)

Nevertheless, excellent adhesion was found at 750°C within 30 s for glass 6P55 (**Figure 5(a)**). This indicates the effect of firing time and temperature on coatings made with glass 6P50 and 6P55, determined by the glass composition and stoichiometry of the glass. From the SEM image (**Figure 5**) different regions were observed, but only four are depicted. Thus, critical time and temperature were the key factors determining the adhesion bond between the two layers of substrate and glass. The glass did not sinter below these values, while at higher temperatures the glass flows and forms a dense layer. The coatings exhibit superior adhesion when both critical temperature and time are considered, resulting in the elimination of delamination and crack propagation on the coated surface.

5. Bonding and Adhesion Strength on a Metallic Substrate

5.1 Adhesion Paradigm and Mechanism of Bioactive Glass to a Metal Substrate

Bioactive glass and metallic substrate adhere better when they have a strong bond. Using strong bond forces between bioactive glass and cobalt-chromium substrate, the deposited bioglass and the substrate are adhered and continuously fused (**Figure 6**). The bonding strength at the primer interface lends itself to increasing the adhesion strength of the adhesive (for example, bioactive glass, paint, inks) that bonds firmly to the substrate even after curing and film formation (94). In general coating processes, whether electrochemical deposition (42) or traditional coatings (paint) (95), various elements influence the adhesion strength, including the nature of the surface (96) (hydrophilic or hydrophobic); surface pre- or post-treatments of the substrate; suspension; and the coating process. The main features of the coating paradigm have been elaborated. Interestingly, all five models outlined in previous studies explain adhesion mechanisms between adhesive and substrate and their physicochemical behaviour. These include (94):

a. Adsorption behaviour is the attraction between surface molecules of two materials adhering at their interfaces through intermolecular forces. They are described by secondary or van der Waals forces that increase molecular contact between them

b. Chemisorption theory defines chemical bonding due to molecular reactions when a treated surface develops affinity to water (96, 97). The chemical bonds formed within the primer interface contribute intrinsically to adhesion and promote functional behaviour to both substrates and adhesive film coatings

c. Mechanical interlocking is defined by the surface roughness of the substrate and glasses' morphology, including their particle size. The affinity of the substrate's surface to water facilitates the molecular interlocking found within the irregularities on its surface, which are small cavities or dents. Thus, controlled surface porosity and porous particles influence the penetration of suspension into cavities, elevating the displacement of trapped air in indented smaller pores on the substrate surface (97, 98)

d. The electrostatics concept defines electrostatic forces within the suspension during EPD (99). The migrating electrons developed during deposition are transferred within the primer from one surface to another, creating a build-up of resistance to delamination. Therefore, the behaviour response *in vivo* application inhibits implant loosening by promoting cell adhesion and particle attachment to the host (4, 100).

In **Figure 6**, different requirements for electrophoretic deposition are illustrated.

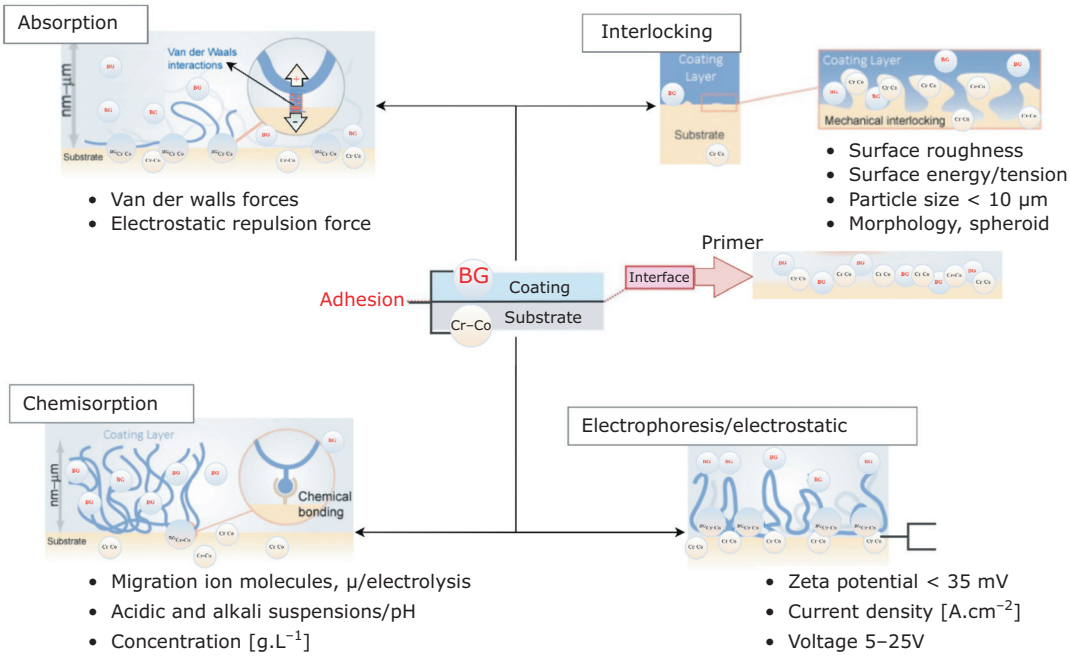

Fig. 6. Adhesion mechanism and theories within the coatings process

Unfortunately, to the best of our knowledge, very few studies have been conducted on the adhesion mechanisms of bioactive glass and cobalt-chromium-based alloys. Some have highlighted adhesion mechanisms using numerical methods and concluded based on experimental observation. Numerous studies have focused on titanium alloys (67) and stainless steels electrophoretically coated by bioactive glasses (74, 101, 102) and bioceramics (81). However, few studies have explored cobalt-based alloys with glasses or bioceramics. This represents a gap in EPD research on biofunctionalised cobalt-based alloys with bioactive glasses for orthopaedic applications. Despite this, a study by Xin *et al.* retouched the mechanics of electrophoresis that induces adhesion by a reversible hydrogel (103). They established an analytical theory framework to model the electrophoresis-induced reversible hydrogel. The theoretical study found the electric force, polymer chain length and chain friction systematically affect the hydrogel adhesion, while the longer process time decreases hydrogel adhesion. This is part of the fifth paradigm of adhesion mechanism theory, contrary to the objective of this study. The concept is diffusion theory, or entanglement behaviour and compatibility of long-chain polymer molecules capable of moving from the coating layer (71) to the substrate and developing an interdiffusion. As a result, the primer surface becomes homogenous and challenging to identify.

The adhesion of polymeric materials penetrates within chains at the polymer interface (71, 104). Studies have defined EPD as a versatile coating technique whereby the electrified particles move within a colloidal solution and are deposited onto the surface of a substrate. The techniques develop a primer interface between the substrate and the migrated particles stick on the surface under adhesion strength and become hard to identify (101). However, the mechanism needs optimum conditions to be fully functionalised. Therefore, after prolonged exposure and post-treatment, different process factors could result in failure (**Table I**). Surface modification by applying a coated layer improves biocompatibility. However, adhesion strength is important. Typically, bone has a low strength ranging between 70–150 MPa compared to 655–1793 MPa of cobalt-based alloys or other metallic materials (**Table IV**) (104–108). Nevertheless, it is superior to those of bioglass ranging from 42 MPa. The bonding strength between bioactive glass and metallic substrates was measured between 15–25 MPa, while bone and inert glass, titanium, cobalt-based alloys and stainless steel were considered very low at 0.5–2 MPa compared to stress shielding exhibited by metal-to-bone due to load transfer from implant to bone (105). According to Liverani *et al.*, the fully dense metal appeared to transfer compressive force subjected to large deformations of 2.2 ± 0.3% strain of 15 kN load stress at the

Table IV Mechanical Properties of Bone Compared to Metallic Materials (99–102)

Material	Tensile strength, MPa	Yield strength, MPa	Elastic modulus, GPa
Bone (cortical)	70–150	30–70	15–30
Bone (limb)	131	104–121	
Stainless steel	490–1350	190–690	200–210
Co-based alloys	655–1793	310–1586	210–253
Titanium-based alloys	690–1100	585–1060	55–110
Dense HA ceramics	40–100	–	70–120
Bioglass 45S5	42	–	35

bone interface (109). Therefore, the mechanical behaviour of such load force resulted in the aseptic failure of orthopaedic implants (110). Thus, the uneven load distribution across the bone normally due to a stiff metal prosthesis component leads to periprosthetic bone resorption (111) and implant loosening (112).

5.2 Coating Paradigm *vs.* Thickness of a Coat

The successful biofunction of a bioglass-coated hip prosthesis or orthopaedic device depends on a solid link between glass and bone and the integrity of glass and metal substrate. However, success of this procedure comes from their biocompatibility and bioactivity in response to the formation of an apatite layer, stimulating new bonelike growth. For example, HA coatings made by plasma spraying (4, 113) or EPD have been extensively investigated (59, 114). Several critical problems are associated with the degradation of HA due to the elevated temperature required during implantation, based on the low CTE of HA leading to a lack of strength at the metal-HA interface (115). To overcome the problem, the literature proposes using bioactive glass that forms HA *in vivo* as an alternative to coating the metal and provides desired bonding attachment to bone (38), similar to the structure of successful biofunctional implants.

Han *et al.* showed an example by investigating gentamicin-loaded silk fibroin coated on a 3D porous cobalt-chromium-molybdenum orthopaedic implant against infections leading to failure (82). They found that mechanical properties aid in reducing undesirable shrinkage behaviour. Similar to the literature, they propose that when customising the shapes of metal bonelike implant biomaterials for patients, the printing process can affect the modulus of materials by designing and manufacturing linked porous structures, thus achieving a modulus that matches the implant and surrounding bone. Therefore, implant longevity can be improved. Unfortunately, porous implants for bone replacements have a far bigger surface area than standard cast solid bone substitutes, which means they are more likely to get infected after surgery (116, 117). Han *et al.* continued their research by coating this porous structure to characterise the coated surface *via* digital and fluorescence microscopy imaging and to analyse the coating quality. The results revealed that the coating was generally intact, continuous, homogenous and conformal with an average thickness of 2.30 ± 0.58 μm, which is negligible compared to the designed strut size of 254.2 ± 18.1 μm, with moderate pore size of 625.0 ± 54.1 μm and with fewer closed pores. These results match well with previous literature, as illustrated in **Figure 7**.

Another method that increases bonding strength was discussed by Lacefield and Hench. They recommended dipping Vitallium® specimens in a solution including glass frit with an appropriate

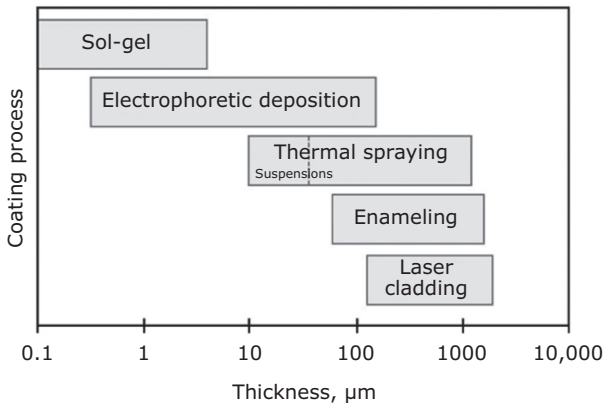

Fig. 7. Coating process over the resulted thickness. Reproduced under the terms of the Creative Commons BY-NC-ND license, from (42)

carrier, then firing the coated rods in an electric furnace (58). The finding was that the glass particles fused and flowed throughout the high-temperature firing cycle and formed a homogenous glass coating. This shows the effect of the sintering conditions. This was demonstrated by an indentation test at the glass-metal interface on a polished cross-section layer. The cracks were not propagated along the interface but tend to be forced into the glass. This shows an incompatibility between coating systems due to the glass composition of 6P50 (38) prepared through the conventional melting method. In their process, the glass NPs were suspended in ethanol and successively deposited on cobalt-chromium alloy plates of Vitallium® 99.0% purity, 15 × 10 × 1 mm, polished with diamond of 1 mm particle size and cleaned in acetone and ethanol. After deposition, the samples were air-dried for 24 h at 75°C to remove organics and heat treated again in air to ensure glass flow and adhesion to the alloy. Their method includes various parameters associated with suspension preparation to obtain a defect-free surface coating.

They also investigated the capability of previously prepared bioglass. The results confirmed that the bioglass developed by Hench has a CTE closer to that of cobalt-chromium alloys (Vitallium®). Consequently, the CTE of various bioactive glasses decreases when incorporating alkaline oxides but softening temperatures increase. This means that the bioglass can be used for coating without generating thermal stress, for example 45S5 Bioglass® (118). However, in the post-heat treatment discussed above, firing (sintering) temperature must be controlled since the bioglass crystallises entirely even at the lowest firing temperature of 700°C, resulting in poor densification and substrate adherence (38). The alkaline oxide that causes bioglass to crystallise early in the firing process should be controlled in the glass composition, including the crystalline phase of sodium-calcium silicate as well as those possessing a hygroscopic nature with more than 20% of alkaline content in glass composition in the presence of OH^- ions on their surface that promote crystallisation at flow temperatures between 600–700°C.

In conclusion, various techniques to identify the surface layer and its bonding adhesion to a metal substrate, like electron microprobe, aid in detecting the extent of diffusion of metallic atoms from the metal into the bioglass coating. Auger electron spectroscopy can characterise glass-metal interfacial regions within a few micrometres of a proper interface. It also aids in finding diffusion gradients and obtaining profiles of elements across the interface. Other techniques include transmission electron microscopy (TEM) or scanning electron microscopy (SEM) for surface morphology and Vickers indentation. As mentioned above, it can be used to identify the adherence of the interface between glass and alloy. In the literature data, simulated body fluid is used to investigate HA formation on the surface for a specified period at 37°C.

5.3 Heat Treatment and Oxidation Time

It has been found that the shear strength increases with increasing oxidation time to a certain point and then decreases. For temperatures above 800°C, the shear strength decreases as oxidation time increases from 5 min and at 350°C, the oxidation time gave a low bond strength regardless of oxidation time. The conclusion was that the optimum oxidation time for each temperature indicates a certain oxide layer thickness that provides maximum bonding strength. Thus, oxidation temperature between 500–650°C is the most suitable for Vitallium, with an oxidation time of 8–15 min depending on the optimum temperature, to coat with the immersion technique (58). Coating with modified immersion techniques such as EPD when the substrate is immersed in a suspension of bioglass NPs may relate to the above studies that compared frit enameling and immersion coating. Hence, the immersion coating process can be considered a primary method to coat bioglass on Vitallium with an average oxidation time of 3 s when the oxides in the glass respect Hamaker's law. The process does not decrease the mechanical properties, which are not affected by heat treatment of the core but gives a smooth, thick glass surface coat without excessive porosity but with good corrosion resistance. Unfortunately, this technique has the drawback of being unable to coat complex shapes in a highly viscous suspension of bioglass NPs at a short immersion time and oxidation time for the NPs to penetrate the internal cavities of the core. This is an advantage of EPD (16, 67).

6. Summary and Outlook

This review has discussed the metallic implant material, cobalt-chromium, EPD coated with bioactive glass, and compared it with other metallic biomaterials. The review also verified

selected techniques like sol-gel (dip and immersion coating), enameling and thermal spraying. Variable parameters that influence coating quality, as found in literature data, affect the resulting surface layer based on the bonding strength between metal and bioglass. During post-heat treatment, densification of bioglass on metallic Vitallium was demonstrated to be possible with controlled time and temperature. Hamaker's law, when respected, improves EPD techniques and the result gives better bonding between bioglass and metal. Different parameters produce functional coatings through EPD with emphasis on post-treatment but mostly on suspension, zeta potential, oxidation time, the surface to coat and temperature incurred in the process.

Thermodilatometric compatibility of bioactive glass coatings with substrate has been found to regulate the formation of harmful thermal stresses at the metal's interface. Heat treatment is carried out at a regulated temperature compared to the expansivity of both materials. This has significant impact on the dependability of the implant. CTE of bioactive glasses must not exceed the CTE of the core. As a general trend, the strong bonds in glass networks undergoing the crystallisation process resulted in small amplitudes and reduced CTE values. Furthermore, the CTE of bioglass must be almost comparable to that of a metal substrate to get acceptable coating layers.

7. Conclusion

In conclusion, the EPD technique gives beneficial functionalities of biological properties for various structures. This includes those with scaffolds and porous materials. Multiple innovative possibilities to modify the interfacial surface of cobalt-chromium and its alloys have been studied. The findings showed optimum regenerative surface inhibition of fast integration of an implant with the host. In addition, EPD parameters such as zeta potential, suspension, pH value, solvent permeability and dielectric field were shown to permit the manipulation and control of micro- and nano-sized coatings. Customising the interfacial surfaces of metallic biomaterials for implant integration and fast regeneration appears feasible in the future for nanoscale coatings with increased nanoparticle bioactivity. Synergistic interdisciplinary studies are required to get a better-biofunctionalised surface.

Acknowledgment

This work was supported by Euromed University of Fez, Morocco (UEMF Research Center) and the Africa Scientific Research and Innovation Council (ASRIC). The authors would like to thank UEMF for their valuable support in making this work possible.

References

1. J. N. Oliver, Y. Su, X. Lu, P.-H. Kuo, J. Du, D. Zhu, *Bioact. Mater.*, 2019, **4**, 261
2. J. Cho, M. Cannio, A. R. Boccaccini, *Int. J. Mater. Prod. Technol.*, 2009, **35**, (3/4), 260
3. R. I. M. Asri, W. S. W. Harun, M. Samykano, N. A. C. Lah, S. A. C. Ghani, F. Tarlochan, M. R. Raza, *Mater. Sci. Eng.: C*, 2017, **77**, 1261
4. A. Dehghanghadikolaei, B. Fotovvati, *Materials*, 2019, **12**, (11), 1795
5. A. Nouri, P. D. Hodgson, C. Wen, 'Biomimetic Porous Titanium Scaffolds for Orthopedic and Dental Applications', in "Biomimetics Learning from Nature", ed. A. Mukherjee, InTech Open Ltd, London, UK, 2010, pp. 415–450
6. Y. Su, I. Cockerill, Y. Zheng, L. Tang, Y.-X. Qin, D. Zhu, *Bioact. Mater.*, 2019, **4**, 196
7. A. Sola, D. Bellucci, V. Cannillo, A. Cattini, *Surf. Eng.*, 2011, **27**, (8), 560
8. J. Liu, N. B. M. Rafiq, L. M. Wong, S. Wang, *Front. Chem*., 2021, **9**, 768007
9. R. A. Gittens, R. Olivares-Navarrete, Z. Schwartz, B. D. Boyan, *Acta Biomater.*, 2014, **10**, (8), 3363
10. B. Priyadarshini, M. Rama, Chetan, U. Vijayalakshmi, *J. Asian Ceram. Soc.*, 2019, **7**, (4), 397
11. K. M. R. Nuss, B. von Rechenberg, *Open Orthop. J.*, 2008, **2**, 66
12. M. Haseeb, M. F. Butt, T. Altaf, K. Muzaffar, A. Gupta, A. Jallu, *Int. J. Health Sci. (Qassim)*, 2017, **11**, (1), 1
13. Q. Chen, J. Jing, H. Qi, I. Ahmed, H. Yang, X. Liu, T. L. Lu, A. R. Boccaccini, *ACS Appl. Mater. Interfaces*, 2018, **10**, (14), 11529
14. A. M. Ballo, O. Omar, W. Xia, A. Palmquist, 'Dental Implant Surfaces –Physicochemical Properties, Biological Performance, and Trends', in "Implant Dentistry – A Rapidly Evolving Practice", ed. I. Turkyilmaz, InTech Open Ltd, London, UK, 2011, pp. 19–56
15. S. V. Dorozhkin, *Acta Biomater.*, 2014, **10**, (7), 2919

16. L. Besra, M. Liu, *Prog. Mater. Sci.*, 2007, **52**, 1
17. S. Seuss, A. Chavez, T. Yoshioka, J. Stein, A. R. Boccaccini, 'Electrophoretic Deposition of Soft Coatings for Orthopaedic Applications', in "Biomaterials Science: Processing, Properties and Applications II: Ceramic Transactions", eds. R. Narayan, S. Bose, A. Bandyopadhyay, Vol. 237, John Wiley & Sons Inc, Hoboken, USA, 2012, pp. 145–152
18. A. Bekmurzayeva, W. J. Duncanson, H. S. Azevedo, D. Kanayeva, *Mater. Sci. Eng.: C*, 2018, **93**, 1073
19. Q. Chen, G. A. Thouas, *Mater. Sci. Eng. R: Rep.*, 2015, **87**, 1
20. Y. F. Zheng, X. N. Gu, F. Witte, *Mater. Sci. Eng. R: Reports*, 2014, **77**, 1
21. C. N. Elias, D. J. Fernandes, F. M. de Souza, E. dos Santos Monteiro, R. S. de Biasi, *J. Mater. Res. Technol.*, 2019, **8**, (1), 1060
22. K. Kuei-Haw-Wang, J. H. Dumbleton, L. J. Gustavson, Pfizer Hospital Products Group Inc, 'Dispersion Strengthened Cobalt-Chromium-Molybdenum Alloy Produced by Gas Atomization', *European Patent* 213,781; 1989
23. 'Cobalt Chrome Chromium Precision Alloy With Good Price', Alibaba Group, Hangzhou, China: https://www.alibaba.com/product-detail/cobalt-chrome-chromium-precision-alloy-with_1045843162.html (Accessed on 11th January 2022)
24. D. J. del Corso, CRS Holding Inc, 'Co-Cr-Mo Powder Metallurgy Articles and Process for Their Manufacture', *US Patent* 5,462,575; 1995
25. A. F. Mavrogenis, P. J. Papagelopoulos, G. C. Babis, *J. Long-Term. Eff. Med. Implants*, 2011, **21**, (4), 349
26. A. Marti, *Injury*, 2000, **31**, (Suppl 4), D18
27. J. Jacobs, A. Skipor, P. Doorn, P. Campbell, T. Schmalzried, J. Black, H. Amstutz, *Clin. Orthop. Relat. Res.*, 1996, **329**, S256
28. C. Lhotka, T. Szekeres, I. Steffan, K. Zhuber, K. Zweymüller, *J. Orthop. Res.*, 2003, **21**, (2), 189
29. A. W. Schaffer, A. Schaffer, A. Pilger, C. Engelhardt, K. Zweymueller, H. W. Ruediger, A. Schaffer, *J. Toxicol: Clin. Toxicol.*, 1999, **37**, (7), 839
30. D. R. Haynes, S. D. Rogers, S. Hay, M. J. Pearcy, D. W. Howie, *J. Bone Joint Surg.*, 1993, **75**, (6), 825
31. Y. Okazaki, E. Gotoh, *Biomaterials*, 2005, **26**, (1), 11
32. M. Navarro, A. Michiardi, O. Castaño, J. A. Planell, *J. R. Soc. Interface*, 2008, **5**, (27), 1137
33. D. Rani Bijukumar, A. Segu, Y. Mou, R. Ghodsi, T. Shokufhar, M. Barba, X.-J. Li, M. Thoppil Mathew, *Nanotoxicology*, 2018, **12**, (9), 941
34. D. Bijukumar, A. Segu, P. Chastain, M. T. Mathew, *Cell Biol. Toxicol.*, 2021, **37**, (6), 833
35. D. R. Bijukumar, A. Segu, J. C. M. Souza, X. J. Li, M. Barba, L. G. Mercuri, J. J. Jacobs, M. T. Mathew, *Nanomed.: Nanotechnol. Biol. Med.*, 2018, **14**, (3), 951
36. B. Green, E. Griffiths, S. Almond, *BMC Psychiatry*, 2017, **17**, 33
37. C. E. Holy, S. Zhang, L. E. Perkins, P. Hasgall, L. B. Katz, J. R. Brown, L. Orlandini, G. Fessel, B. Nasseri-Aghbosh, G. Eichenbaum, N. S. Egnot, S. Marcello, P. M. Coplan, *Regul. Toxicol. Pharmacol.*, 2022, **129**, 105096
38. S. Fujino, H. Tokunaga, E. Saiz, A. P. Tomsia, *Mater. Trans.*, 2004, **45**, (4), 1147
39. G. Genchi, A. Carocci, G. Lauria, M. S. Sinicropi, A. Catalano, *Int. J. Environ. Res. Public Health*, 2020, **17**, (3), 679
40. Z. Guo, X. Pang, Y. Yan, K. Gao, A. A. Volinsky, T.-Y. Zhang, *Appl. Surf. Sci.*, 2015, **347**, 23
41. D. Bellucci, V. Cannillo, A. Sola, *Ceram. Int.*, 2011, **37**, (8), 2963
42. B. Garrido, S. Dosta, I. G. Cano, *Bol. Soc. Esp. Ceram. Vidr.*, 2021, **61**, (5), 516
43. A. Kirsten, A. Hausmann, M. Weber, J. Fischer, H. Fischer, *J. Dent. Res.*, 2015, **94**, (2), 297
44. J. Fischer, B. Stawarczyk, M. Tomic, J. R. Strub, C. H. F. Hämmerle, *Dent. Mater. J.*, 2007, **26**, (6), 766
45. A. G. Evans, G. B. Crumley, R. E. Demaray, *Oxid. Met.,* 1983, **20**, (5–6), 193
46. "Biomedical Materials", ed. R. Narayan, Springer Science and Business Media LLC, New York, USA, 2009, 566 pp
47. M. M. Babu, P. S. Prasad, S. H. Bindu, A. Prasad, P. V. Rao, N. P. Govindan, N. Veeraiah, M. Özcan, *J. Compos. Sci.*, 2020, **4**, (3), 129
48. P. Anigrahawati, M. R. Sahar, S. K. Ghoshal, *Mater. Chem. Phys.*, 2015, **155**, 155
49. S. Kapoor, A. Goel, A. F. Correia, M. J. Pascual, H.-Y. Lee, H.-W. Kim, J. M. F. Ferreira, *Mater. Sci. Eng.: C,* 2015, **53**, 252
50. L. Zhang, S. Liu, *J. Non-Cryst. Solids*, 2017, **473**, 108
51. M. J. Jackson, B. Mills, *J. Mater. Sci. Lett.*, 1997, **16**, (15), 1264
52. A. Fluegel, *Glass Technol. – Eur. J. Glass Sci. Technol. Part A*, 2010, **51**, (5), 191
53. M. D. O'Donnell, *Acta Biomater.*, 2011, **7**, (5), 2264
54. L. L. Hench, *J. Mater. Sci.: Mater. Med.*, 2006, **17**, (11), 967
55. T. Parry, B. Fitzsimons, 'Coating Failures and Defects: A Comprehensive Field Guide', Corrosionpedia, Janalta Interactive Inc,

Edmonton, Canada, 46 pp: https://www.corrosionpedia.com/14/5351/coatings-and-lining/coating-failures-and-defects-guide (Accessed on 3rd January 2022)

56. C. K. Schoff, 'Automotive Coatings: Application Defects', American Coatings Association, Washington, DC, USA: https://www.paint.org/coatingstech-magazine/articles/automotive-coatings-application-defects/ (Accessed on 3rd January 2022)
57. R. Talbert, 'Porosity Causes on Powder – Coated Surfaces', Products Finishing, Cincinnati, USA: https://www.pfonline.com/articles/cause-of-porosity (Accessed on 3rd January 2022)
58. W. R. Lacefield, L. L. Hench, *Biomaterials*, 1986, **7**, (2), 104
59. M. Farrokhi-Rad, S. K. Loghmani, T. Shahrabi, S. Khanmohammadi, *J. Eur. Ceram. Soc.*, 2014, **34**, (1), 97
60. B. Henriques, M. Gasik, J. C. M. Souza, R. M. Nascimento, D. Soares, F. S. Silva, *J. Mech. Behav. Biomed. Mater.*, 2014, **30**, 103
61. Y. Li, H. Jahr, J. Zhou, A. A. Zadpoor, *Acta Biomater*., 2020, **115**, 29
62. S. Singh, G. Singh, N. Bala, *Mater. Today: Proc.*, 2018, **5**, (9), Part 3, 20160
63. Z. Tabia, M. Bricha, K. El Mabrouk, S. Vaudreuil, *J. Mater. Sci.*, 2021, **56**, (2), 1658
64. L. L. Hench, H. A. Paschall, *J. Biomed. Mater. Res.*, 1973, **7**, (3), 25
65. M. N. Rahaman, D. E. Day, B. S. Bal, Q. Fu, S. B. Jung, L. F. Bonewald, A. P. Tomsia, *Acta Biomater.*, 2011, **7**, (6), 2355
66. B. D. de Greñu, R. de los Reyes, A. M. Costero, P. Amorós, J. V. Ros-Lis, *Nanomaterials*, 2020, **10**, (6), 1092
67. I. Azzouz, J. Faure, K. Khlifi, A. C. Larbi, H. Benhayoune, *Coatings*, 2020, **10**, (12), 1192
68. P.-H. Kuo, S. S. Joshi, X. Lu, Y.-H. Ho, Y. Xiang, N. B. Dahotre, J. Du, *Int. J. Appl. Glass Sci.*, 2019, **10**, (3), 307
69. D. Krause, B. Thomas, C. Leinenbach, D. Eifler, E. J. Minay, A. R. Boccaccini, *Surf. Coatings Technol.*, 2006, **200**, (16–17), 4835
70. F. Pishbin, V. Mouriño, S. Flor, S. Kreppel, V. Salih, M. P. Ryan, A. R. Boccaccini, *ACS Appl. Mater. Interfaces*, 2014, **6**, (11), 8796
71. S. A. Batool, A. Wadood, S. W. Hussain, M. Yasir, M. A. Ur Rehman, *Surfaces*, 2021, **4**, (3), 205
72. M. H. Fathi, A. Doostmohammadi, *J. Mater. Process. Technol.*, 2009, **209**, (3), 1385
73. A. Cattini, D. Bellucci, A. Sola, L. Pawłowski, V. Cannillo, *J. Biomed. Mater. Res.: B.: Appl. Biomater.*, 2014, **102**, (3), 551
74. M. Miola, E. Verné, F. E. Ciraldo, L. Cordero-Arias, A. R. Boccaccini, *Front. Bioeng. Biotechnol.*, 2015, **3**, 1
75. T. Distler, N. Fournier, A. Grünewald, C. Polley, H. Seitz, R. Detsch, A. R. Boccaccini, *Front. Bioeng. Biotechnol.*, 2020, **8**, 552
76. I. Bagherpour, S. M. Naghib, A. H. Yaghtin, *IET Nanobiotechnol.*, 2018, **12**, (7), 895
77. Y. S. Joung, C. R. Buie, Massachusetts Institute of Technology, 'Electrophoretic-Deposited Surfaces', *US Patent* 9,096,942; 2015
78. L. Cordero-Arias, S. Cabanas-Polo, J. Gilabert, O. M. Goudouri, E. Sanchez, S. Virtanen, A. R. Boccaccini, *Adv. Appl. Ceram.*, 2014, **113**, (1), 42
79. V. O. Kollath, Q. Chen, S. Mullens, J. Luyten, K. Traina, A. R. Boccaccini, R. Cloots, *J. Mater. Sci.*, 2016, **51**, (5), 2338
80. M. Farhadian, K. Raeissi, M. A. Golozar, S. Labbaf, T. Hajilou, A. Barnoush, *Surf. Coat. Technol.*, 2019, **380**, 125015
81. M. R. Shirdar, S. Izman, H. M. K. N. Ahmad, A. Ma'aram, *Surf. Innov.*, 2017, **5**, (2), 90
82. C. Han, Y. Yao, X. Cheng, J. Luo, P. Luo, Q. Wang, F. Yang, Q. Wei, Z. Zhang, *Biomacromolecules*, 2017, **18**, (11), 3776
83. S. Seuss, M. Lehmann, A. R. Boccaccini, *Int. J. Mol. Sci.*, 2014, **15**, (7), 12231
84. D. Hanaor, M. Michelazzi, P. Veronesi, C. Leonelli, M. Romagnoli, C. Sorrell, *J. Eur. Ceram. Soc*., 2011, **31**, (6), 1041
85. Y. Su, I. Zhitomirsky, *J. Colloid Inteface Sci*., 2013, **399**, 46
86. 'An Introduction to Zeta Potential in 30 Minutes', Zetasizer Nano Series Technical Note MRK 654-01, Malvern Panalytical Ltd, Malvern, UK, 2011
87. K. Ma, D. Huang, J. Cai, X. Cai, L. Gong, P. Huang, Y. Wang, T. Jiang, *Colloids Surf. B: Biointerfaces*, 2016, **146**, 97
88. M. Diba, D. W. H. Fam, A. R. Boccaccini, M. S. P. Shaffer, *Prog. Mater. Sci.*, 2016, **82**, 83
89. Y. Ahmed, A. Nawaz, R. S. Virk, A. Wadood, M. A. U. Rehman, *Int. J. Ceram. Eng. Sci.*, 2020, **2**, (5), 254
90. M. S. Safavi, F. C. Walsh, M. A. Surmeneva, R. A. Surmenev, J. K.-Allafi, *Coatings*, 2021, **11**, (1), 110
91. M. Sari, N. A. Kristianto, Chotimah, I. D. Ana, Y. Yusuf, *Coatings*, 2021, **11**, (8), 941
92. A. R. Boccaccini, F. Chicatun, J. Cho, O. Bretcanu, J. A. Roether, S. Novak, Q. Z. Chen, *Adv. Funct. Mater.*, 2007, **17**, (15), 2815
93. A. R. Boccaccini, S. Keim, R. Ma, Y. Li,

I. Zhitomirsky, *J. R. Soc. Interface*, 2010, **7**, (5), S581

94. 'Adhesion in Paint and Coatings', SpecialChem, Paris, France: https://coatings.specialchem.com/coatings-properties/adhesion (Accessed on 1st November 2022)
95. I. O. Owate, C. W. I. Ezi, G. Avwiri, *J. Appl. Sci. Environ. Manag.*, 2002, **6**, (2), 79
96. H. Moghadas, M. S. Saidi, N. Kashaninejad, A. Kiyoumarsioskouei, N.-T. Nguyen, *Biomed. Microdevices*, 2017, **19**, (4), 74
97. M. K. Abbass, M. J. Khadhim, A. N. Jasim, M. J. Issa, *J. Phys.: Conf. Ser.*, 2021, **1773**, 012035
98. J.-Y. Hong, S.-Y. Ko, W. Lee, Y.-Y. Chang, S.-H. Kim, J.-H. Yun, *Materials*, 2020, **13**, (14), 3061
99. J. J. Van Tassel, C. A. Randall, *Key Eng. Mater.*, 2006, **314**, 167
100. S. V. Dorozhkin, *Adv. Nano-Bio-Mater. Dev.*, 2019, **3**, (4), 422
101. K. Kawaguchi, M. Iijima, K. Endo, I. Mizoguchi, *Coatings*, 2017, **7**, (11), 199
102. M. Miola, L. Cordero-Arias, G. Ferlenda, A. Cochis, S. Virtanen, L. Rimondini, E. Verné, A. R. Boccaccini, *Surf. Coatings Technol.*, 2021, **418**, 127183
103. A. Xin, R. Zhang, K. Yu, Q. Wang, *J. Mech. Phys. Solids*, 2019, **125**, 1
104. A. Nawaz, M. A. Ur Rehman, *J. Appl. Polym. Sci.*, 2021, **138**, (15), 50220
105. J. Folgado, P. R. Fernandes, 'Bone Tissue Mechanics', Biomecânica dos Tecidos, Instituto Superior Tecnico, Lisbon, Portugal, 2015
106. 'Bone Density Scan', MedlinePlus, National Library of Medicine, Bethesda, USA, 2020: https://medlineplus.gov/lab-tests/bone-density-scan/ (Accessed on 26th March 2021)
107. E. Chlebus, B. Kuźnicka, T. Kurzynowski, B. Dybała, *Mater. Charact.*, 2011, **62**, (5), 488
108. Y. Li, H. Jahr, K. Lietaert, P. Pavanram, A. Yilmaz, L. I. Fockaert, M. A. Leeflang, B. Pouran, Y. Gonzalez-Garcia, H. Weinans, J. M. C. Mol, J. Zhou, A. A. Zadpoor, *Acta Biomater.*, 2018, **77**, 380
109. E. Liverani, G. Rogati, S. Pagani, S. Brogini, A. Fortunato, P. Caravaggi, *J. Mech. Behav. Biomed. Mater.*, 2021, **121**, 104608
110. J. Adhikari, P. Saha, A. Sinha, 'Surface Modification of metallic bone implants –Polymer and Polymer-Assisted Coating for Bone In-Growth', in "Fundemental Biomaterials: Metals", eds. P. Balakrishnan, M. S. Sreekala, S. Thomas, Ch. 14, Elsevier Ltd, Duxford, UK, 2018, pp. 299–321
111. R. B. Kahla, A. Barkaoui, 'Bone Multiscale Mechanics', in "Bone Remodelling Process: Mechanics, Biology, and Numerical Modeling", Elsevier Inc, San Diego, USA, 2021, pp. 1–47
112. P. Sahoo, S. K. Das, J. Paulo Davim, 'Tribiology of Materials for Biomedical Applications', in "Mechanical Behaviour of Biomaterials", ed. J. P. Davim, Woodhead Pulishing Series in Biomaterials, Ch. 1, Elsevier Ltd, Duxford, UK, 2019, pp. 1–45
113. B. Singh, G. Singh, B. S. Sidhu, *J. Therm. Spray Technol.*, 2018, **27**, (8), 1401
114. M. Djošić, A. Janković, V. Mišković-Stanković, *Materials,* 2021, **14**, (18), 5391
115. W. R. Lacefield, *Ann. N. Y. Acad. Sci.*, 1988, **523**, (1), 72
116. K. B. Hazlehurst, C. J. Jiang, M. Stanford, *Mater. Des.*, 2014, **60**, 177
117. K. Hazlehurst, C. J. Wang, M. Stanford, *Mater. Des.*, 2013, **51**, 949
118. F. Baino, S. Hamzehlou, S. Kargozar, *J. Funct. Biomater.*, 2018, **9**, (1), 25
119. O. van der Biest, S. Put, G. Anné, J. Vleugels, *J. Mater. Sci.*, 2004, **39**, (3), 779
120. J. Zhou, H. He, Z. Shi, G. Liu, C.-W. Nan, *J. Appl. Phys.*, 2006, **100**, (9), 094106

The Authors

Patrick Munyensanga is a PhD student at the Euromed University of Fez, specialising in biomaterials and additive manufacturing. His research primarily centres on porous implants for bone regeneration. He is also profoundly interested in smart manufacturing, additive manufacturing and advanced nanocoating applications to improve biocorrosion resistance in additively manufactured porous metallic structures. He holds a Master of Engineering from Diponegoro University, Indonesia, and a Bachelor of Science in Engineering from the University of Rwanda, focusing on mechanical and materials engineering.

Meriame Bricha obtained her Doctorate in Physico-Chemical Materials, Ceramics and Nanocomposites at the Faculty of Sciences of Agdal in Rabat, Morocco, in 2013, in collaboration with Ceramic Biomaterials Center at iNANOTECH (MAScIR), Rabat. She is Associate Professor at The Euromed Polytechnic School, Euromed University of Fez. Her research interests are ceramics, bioglass and the biocorrosion of parts from metal additive manufacturing by SLM after surface treatment by electrophoretic deposition for bone tissue regeneration.

Khalil El Mabrouk obtained his PhD in Chemical Engineering in 2005 at Laval University, Canada; postdoctoral research at Queen's University, Canada and Dow Chemical New Jersey, USA. He was Research Director in the Moroccan Foundation for Advanced Science Innovation and Research from 2008 to 2013. Since 2013 he is Full Professor at The Euromed Polytechnic School, Euromed University of Fez, Morocco. His research interests are additive manufacturing, soft and hard tissue engineering, bone regeneration, wound healing and advanced materials for medical and aerospace applications.